

# Stretchable Self-Healing Polymeric Networks with Recyclability and Dual Responsiveness

Xingyi Dai, Yuzhang Du, Yansong Wang,\* Yuncong Liu, Nianxi Xu, Yifan Li, Dongzhi Shan, Ben Bin Xu, and Jie Kong\*



Cite This: *ACS Appl. Polym. Mater.* 2020, 2, 1065–1072



Read Online

ACCESS |



Metrics & More



Article Recommendations



Supporting Information

**ABSTRACT:** Intelligent polymers with tough networks are of considerable significance for the development of highly proficient polymer science and technology. In this work, polymeric elastomers with integrated stretchable and self-healable characteristics were designed by cross-linking hyperbranched polymers with flexible segments. The hyperbranched polymer with multiple terminal groups provided various cross-linking points so that mechanically robust networks could be achieved. Driven by the reversibility of imine and disulfide bonds employed, the elastomers exhibited good self-healing property, and the healing efficiency reached up to 99% under ambient environments. Furthermore, the dynamic reversibility of the polymers was investigated at the molecular level. The imine and disulfide bonds were incorporated into the networks to construct a soluble and recyclable hyperbranched polymer with pH and redox responsiveness via an  $A_2 + B_3$  approach and Schiff base polymerization. The polymers containing imine bonds completed the polymerization–depolymerization transition and underwent reversible cycles several times through changing pH. Moreover, in the presence of disulfide bonds, the polymers were provided with a redox cleavage property triggered by dithiothreitol. This study provides new opportunities for the design and application of intelligent polymers with tough networks through regulation of topological structures.

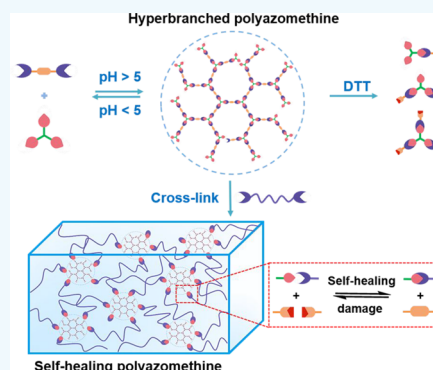
**KEYWORDS:** reversible covalent bonds, hyperbranched polymers, stretchable, recyclable, self-healing

## INTRODUCTION

Dynamic covalent bonds (DCB),<sup>1–3</sup> which can be dissociated and regenerated with changed environmental factors, including temperature, pressure, and pH, have received dramatic interest. This adaptability offers great potential for developing functional materials through the utilization of DCB.<sup>4,5</sup> Thermally activated alkoxyamine bonds,<sup>6,7</sup> pH-sensitive imines,<sup>8–10</sup> acylhydrazone bonds,<sup>11–13</sup> redox and visible light-induced diselenide bonds,<sup>14</sup> thermally reversible Diels–Alder reactions,<sup>15,16</sup> and multiresponsive disulfide bonds triggered under pH, light, and redox conditions<sup>17–19</sup> can all be used as reversible covalent bonds.<sup>20</sup> If the DCB is employed to construct polymeric networks, the resulting dynamic networks or dynamic polymers can be endowed with fascinating smart properties. It is well-known that the main objective of the emphasis on traditional polymer design is to enhance thermal, mechanical, electrical, optical, magnetic, or chemical properties and prevent the cleavage of bonds in case the performance deteriorates. Once the chemical bonds are broken, they may lose the practical value because the irreversible bonds are not repairable. Unlike traditional polymers, however, the dynamic networks or dynamic polymers with reversible characteristics can reorganize or optimize the networks upon exposure to stimulus and be adaptable to environmental change through

the cleavage and recombination of the reversible covalent bonds.<sup>4,21</sup> Therefore, the self-healable and recyclable polymers containing DCB are attractive because they can be regenerated with functionalities recovered and extend usage lifetime and reduce environmental burden.<sup>21–24</sup>

As one of the dynamic bonds, imine bond ( $C=N$ ) is easily formed from an amine and an aldehyde under weakly acidic environments.<sup>25,26</sup> The imine bonds generated from aromatic amine and aromatic aldehyde are more stable than their aliphatic counterparts. However, the generation of a lot of benzene in polymeric architecture leads to the rigid backbone, which may render the polyazomethine<sup>27,28</sup> poorly soluble, thus limiting its applications in many fields. On the other hand, the rigid structure can be used to regulate the mechanical properties of polymers associated with moderate soft segments. Further, the disulfide bond is also attractive due to its merits in



**Special Issue:** Toughening of Networks and Gel Through Molecular Design

**Received:** November 10, 2019

**Accepted:** January 31, 2020

**Published:** February 10, 2020

facile operation, easily available raw materials, and multiple stimuli-responsiveness.

Nowadays, various topological structures such as linear,<sup>29</sup> cross-linked,<sup>30</sup> dendritic,<sup>31</sup> hyperbranched,<sup>32</sup> star-shaped,<sup>33</sup> brush-shaped,<sup>34</sup> and polyrotaxane networks<sup>35</sup> are widely applied to constructing polymeric networks. Notably, hyperbranched polymers show a great deal of special features such as low intrinsic viscosity, low interchain entanglements, excellent solubility, and the existence of multifunctional groups.<sup>36–38</sup> Therefore, if hyperbranched architecture is incorporated into polyazomethine, a type of soluble polyazomethine with good performance could be achieved. Moreover, taking advantage of hyperbranched structure with large number of terminal groups, robust cross-linking networks can be easily constructed. The investigation opens up new avenues for designing dynamic polymers and networks with ideal structures for applications in self-healing materials, molecular logical gate,<sup>39,40</sup> programmable polymers,<sup>41,42</sup> and recyclable and sustainable materials.<sup>43</sup>

In this work, the reversible imine and disulfide bonds were combined to prepare the hyperbranched polymer with intelligent dynamic response characteristics, and the stretchable self-healing polymeric networks were designed benefiting from the special features of hyperbranched architecture. Herein, the dynamic hyperbranched polyazomethine (hb-PAM) with terminal aldehyde groups and good solubility was synthesized via an  $A_2 + B_3$  approach. At the molecular level, the dynamic reversibility of hb-PAM was systematically investigated. For the pH-sensitivity of the imine bond, hb-PAM realized polymerization–depolymerization transition several times. Meanwhile, hb-PAM containing a disulfide bond was endowed with redox cleavage property. Further, hb-PAM could be further cross-linked with soft segments to achieve stretchable and tough self-healing polyazomethine (SH-PAM). SH-PAM exhibited good elasticity and self-recovery capability. Moreover, the mechanical performances of SH-PAM elastomers were tunable to obtain polymeric networks with high strength or stretchability. Remarkably, SH-PAM elastomers were demonstrated to present excellent self-healing property and dual responsiveness.

## EXPERIMENTAL SECTION

**2.1. Materials.** Trimethylolethane (TME, 98.0%), *p*-toluenesulfonylchloride (TsCl, 99.0%), and 4,4'-dithiodianiline (98.0%) were purchased from TCI (Shanghai) Development Co., Ltd. 4-Hydroxybenzaldehyde (99.0%), potassium carbonate (99%), dithiothreitol (DTT, 99%), and poly(propylene glycol)bis(2-aminopropyl ether) 2000 (PEA 2000) were provided by Aladdin Shanghai Co. All reagents were used as received without further purification.

**2.2. Synthesis of Hyperbranched Polyazomethine.** 1,1,1-Tris[(4-formylphenoxy)methyl]ethane (FPME) was synthesized using a previously reported method<sup>9</sup> with a small improvement (see the details in Supporting Information). FPME (0.290 g, 0.6 mmol) was completely dissolved in *N,N*-dimethylformamide (DMF, 10 mL), followed by addition of glacial acetic acid (AcOH, 60  $\mu$ L, 0.3% v/v) as an acid catalyst. Then, 4,4'-dithiodianiline (0.152 g, 0.6 mmol) dissolved in anhydrous DMF (10 mL) was added dropwise to the solution for over 1 h. The mixture was further reacted at 25 °C under nitrogen atmosphere for 26 h. After DMF was evaporated, the mixture was redissolved in tetrahydrofuran (THF, 5 mL) and subsequently added dropwise into methanol (60 mL) with stirring. The formed precipitate was collected and dried in vacuum at 35 °C. Eventually, the yellow powders of hyperbranched polyazomethine (hb-PAM) were obtained (0.388 g, 92.3%).

**2.3. Reversibility of Imine Bonds.** The hb-PAM was dissolved in DMF, followed by addition of hydrochloric acid (HCl, 1% v/v) to the solution to cleave hb-PAM. After a certain time, HCl was saturated with equivalent amount of triethylamine (NET<sub>3</sub>), which resulted in the formation of the salts of HCl and NET<sub>3</sub>. Then, the demonomers were extracted with dichloromethane. Subsequently, the solvent was evaporated. To regenerate hyperbranched polyazomethine hb-PAMC 1, the purified demonomers were dissolved in DMF, to which AcOH (0.3% v/v) was added. The reaction conditions of hb-PAMC 1 were same as those of hb-PAM. After the reaction, a part of hb-PAMC 1 and residual monomers were extracted with dichloromethane, from which the AcOH and DMF were removed with water. The remaining solution was used for the next step. In the same way, imine linkage was constantly broken and reformed, and correspondingly, hyperbranched polyazomethines hb-PAMC 2 to hb-PAMC 4 were obtained.

**2.4. Reduction Degradation of Hyperbranched Polyazomethine.** The hb-PAM (5 mg) and DTT (15 mg) were dissolved in THF (1 mL, in flask) with stirring under nitrogen atmosphere at room temperature to start disulfide degradation in the polymer.

**2.5. Preparation of Self-Healing Polyazomethine.** Typically, FPME was dissolved in anhydrous DMF, which was followed by the addition of AcOH (0.3% v/v). Then, 4,4'-dithiodianiline dissolved in DMF was added dropwise over 1 h. The mixture was further reacted at 25 °C under nitrogen atmosphere for 26 h. Subsequently, PEA dissolved in DMF was added to the solution. After the mixture was further reacted for 12 h, the solution was cast into a Teflon mold. Finally, the resulting polymer was put into an oven at 40, 50, and 60 °C for 3 days. Two kinds of self-healing polyazomethine (SH-PAM-1 and SH-PAM-2) were prepared according to the above methods. The molar ratios of FPME, 4,4'-dithiodianiline, and PEA were 2:2:1 and 2:1:2 for SH-PAM-1 and SH-PAM-2, respectively.

**2.6. Characterizations.** Nuclear magnetic resonance (NMR) analyses were performed on a Bruker Avance 400 spectrometer (Bruker Biospin, Switzerland). The deuterated dimethyl sulfoxide (DMSO-*d*<sub>6</sub>) and deuterated chloroform (CDCl<sub>3</sub>) were used as solvents. Fourier transform infrared (FTIR) spectroscopy analyses were recorded on an FTIR spectrophotometer (PerkinElmer, United States). The ultraviolet–visible spectra (UV–vis) were obtained using a Shimadzu UV2550 UV–vis spectrophotometer (Shimadzu UV2550, Japan). Molecular weight and molecular weight distribution were measured using size exclusion chromatography (SEC) with multiangle laser light scattering systems (MALLS, DAWN EOS, Wyatt, United States) equipped with a Waters 515 pump, an autosampler, and two MZ gel columns (103 and 104 Å). The flow rate was 0.5 mL min<sup>-1</sup> in THF (HPLC grade) at 25 °C. The refractive index increments of polymers in THF were measured at 25 °C on a differential refractometer (OptilabREX, Wyatt, United States). The mechanical tensile tests (dumbbell shaped specimens, 12 mm × 2 mm × 0.8 mm) were performed using an Instron E1000 all-electric dynamic test instrument with a stretching speed of 20 mm min<sup>-1</sup> according to ISO37-4 standard.

## RESULTS AND DISCUSSION

**3.1. Synthesis of Hyperbranched Polyazomethine.** The synthesis process of hb-PAM is exhibited in Figure 1. It could be obtained via Schiff base polymerization between amino groups of 4,4'-dithiodianiline ( $A_2$ ) and aldehyde groups of FPME ( $B_3$ ). Commonly, gelation easily occurs in  $A_2 + B_3$  system; however, it is important to control the reaction conditions. Herein, the rate of reaction was controlled by slowly adding  $A_2$  monomer to  $B_3$  monomer in dilute solution as well as a catalytic amount of acid. Moreover, the molar ratio of the reactive monomers was adjusted to 1:1. By taking these factors into account, a type of hyperbranched polymer based on imine bond (hb-PAM) with excellent solubility was successfully synthesized.

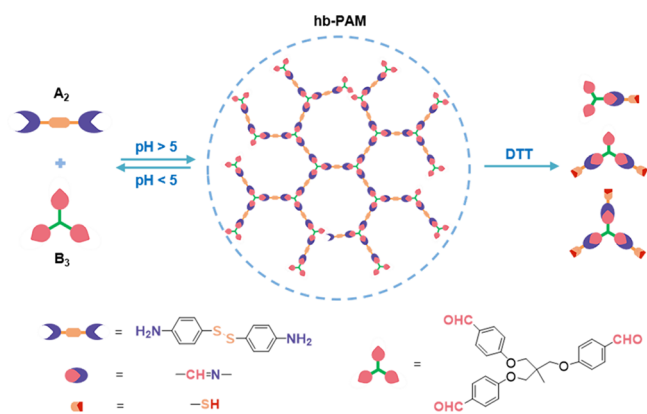


**Figure 1.** Schematic illustration of synthesis of hyperbranched polymer (hb-PAM) based on imine and disulfide bonds with reversible pH and redox responsiveness.

The structure of hb-PAM was identified by FTIR and  $^1\text{H}$  NMR spectroscopy. As shown in Figure 2, compared to the

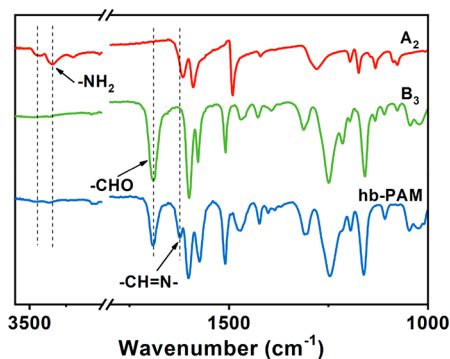


**Figure 2.** FTIR spectra of  $A_2$  monomer (4,4'-dithiodianiline),  $B_3$  monomer (1,1-tris[(4-formylphenoxy)methyl]ethane), and hb-PAM between 3600–1000  $\text{cm}^{-1}$ .

monomers, a new peak appears at  $1624\text{ cm}^{-1}$  for hb-PAM, attributed to the generation of an imine bond ( $\text{CH}=\text{N}$ ). Moreover, the two broad peaks in the range of  $3300\text{--}3700\text{ cm}^{-1}$  resulted from amine groups almost disappear, and a peak at  $1680\text{ cm}^{-1}$  assigned to carbonyl ( $\text{C}=\text{O}$ ) becomes weaker, indicating the successful synthesis of hb-PAM with terminal aldehyde groups ( $\text{CHO}$ ). Figure 3a exhibits  $^1\text{H}$  NMR spectra of hb-PAM, where the appearance of the peak at  $8.37\text{ ppm}$  further validates the formation of an imine bond. Furthermore, a weak peak at  $6.70\text{ ppm}$  ascribed to the protons of benzene near the amine reveals the presence of a few unreacted amine groups resulting from steric hindrance. The proton peak of the end aldehyde groups is also observed at  $9.91\text{ ppm}$ . In addition, the  $M_{w,\text{SEC}}$  of hb-PAM is  $19\,600\text{ g mol}^{-1}$ , and the PDI is 1.53 (Table 1). The increased molecular weight evidently demonstrated the polycondensation. The MALLS is an effective technique for determining the absolute molar mass, thus the combination of SEC with MALLS analysis could avoid the mismatch between hyperbranched architecture and linear polystyrene calibration in normal SEC technology.

**3.2. Reversibility of Imine Bonds.** The formation of imine bond could be accelerated by adding a small amount of acid. At low pH, however, the imine linkage was cleaved.<sup>10</sup> Therefore, the polymer containing the imine bond could be decomposed into monomers under the acidic conditions, and

the demonomers could polymerize again to generate polymer via regulating the reaction conditions as shown in Figure 1. The pH responsive cleavage of hb-PAM was investigated first. When the apparent pH was adjusted to 4–5 by adding HCl (1% v/v) to the solution of hb-PAM, the decomposition of imine bonds occurred. Moreover, the polymer degraded into monomers over time. The demonomers were extracted with dichloromethane and washed with water to remove residual HCl and some other impurities to avoid any adverse effect on the subsequent reaction. The cleavage of hb-PAM was examined by  $^1\text{H}$  NMR spectroscopy and SEC-MALLS. Figure 3b presents  $^1\text{H}$  NMR spectra of purified demonomers in  $d_6$ -DMSO. Compared to the spectra of hb-PAM, the proton peak of imine at  $8.52\text{ ppm}$  becomes much weaker; the proton peak at  $9.86\text{ ppm}$  corresponding to the terminal aldehyde groups is relatively strong, and the proton peak of amine groups at  $5.50\text{ ppm}$  appears. The residual proton peak of imine resulted from high reactivity between amine and aldehyde groups as well as the reversibility of the reaction. Figure 4 shows the SEC trace of the demonomers, revealing that the time of appearance of the peak was much later than that of hb-PAM, and the distinct bimodal distribution could be observed, indicating the presence of two monomers and some oligomers. The dependence of cleavage of the imine bond on time was further investigated in THF, and the pH value of the solution was adjusted to about 5 by addition of AcOH. The reproduced UV–visible absorption spectral curves of hb-PAM measured in various time intervals were obtained as depicted in Figure 3c. Clearly, intensity of the absorption band at around  $338\text{ nm}$ , corresponding to conjugated imine, decreases with time. After 9 h, the system reached equilibrium. These results demonstrated that the imine bond could be cleaved when the pH is below 5.0.

Then, the demonomers regenerating hyperbranched polyazomethine and the transition process of polymer and demonomers were explored. The demonomers were still highly active to polymerize, forming hb-PAMC 1 under the mild reaction conditions same as that of hb-PAM. Herein, the transition process of polymer and demonomers was repeated for four circles in one system, and the corresponding polymers (hb-PAMC 2, hb-PAMC 3, hb-PAMC 4) were obtained. Each time the polymer was depolymerized, the results were monitored by  $^1\text{H}$  NMR spectroscopy. As shown in Figure 3b, the  $^1\text{H}$  NMR spectra of demonomers (MD 1–4) are almost the same, and all peaks at  $8.52\text{ ppm}$  assigned to the imine proton  $\text{CH}=\text{N}$  become weak, indicating that the depolymerization to monomers was successfully triggered at low pH. Figure 3a presents that the  $^1\text{H}$  NMR spectra of hb-PAM and hb-PAMC 2–4 remain almost the same, and the characteristic signals of proton on  $\text{CH}=\text{N}$  bond ( $8.37\text{ ppm}$ ) grow stronger. Moreover, in the SEC traces, the peaks of hb-PAM and hb-PAMC 2–4 appear almost at the same time at about 12 min (elution time) as shown in Figure S4 in Supporting Information. The similarity of the traces might be coincidental and more variation would be expected if these experiments were repeated. The corresponding molecular weights of the cyclic hb-PAMs are summarized in Table 1. Figure 3d depicts relatively small change in weight-average molecular weight with cyclic times for hb-PAM and hb-PAMC 2–4. After the dissociation of hb-PAM, the demonomers still have the ability to polymerize to regenerate the hyperbranched polymer with high molecular weight close to that of the original polymer hb-PAM. The results indicate that the

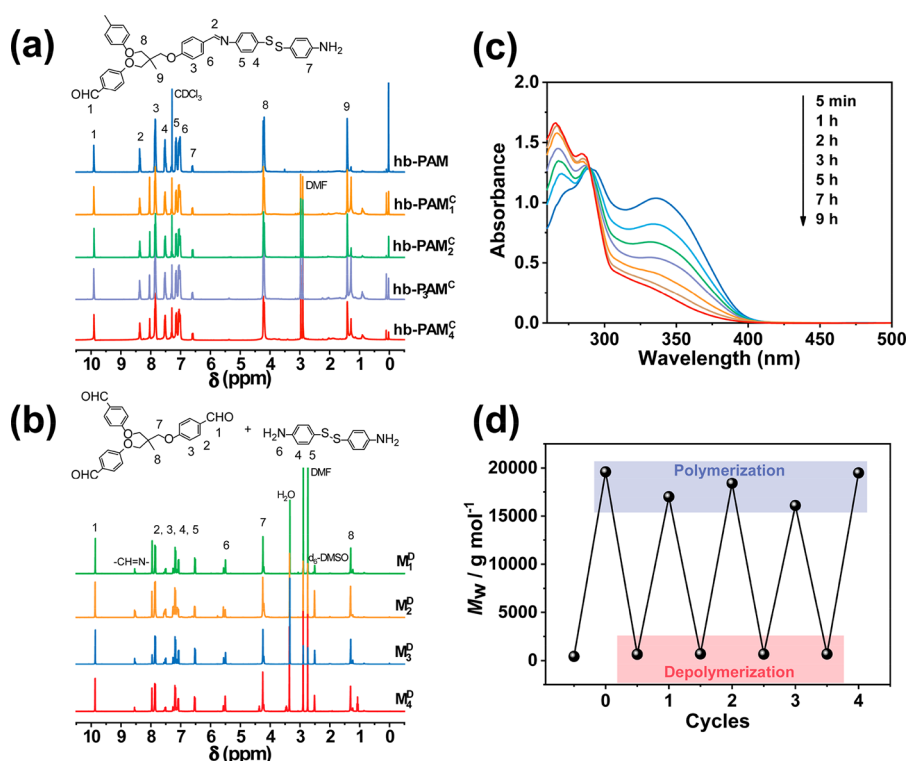


**Figure 3.** (a) <sup>1</sup>H NMR spectra of hyperbranched polyazomethines in CDCl<sub>3</sub>. (b) <sup>1</sup>H NMR spectra of monomers in d<sub>6</sub>-DMSO, (c) UV-visible absorption spectra of hb-PAM obtained at various time intervals at pH 5. (d) Change in average molecular weight of hyperbranched polyazomethines for four cycles of depolymerization–repolymerization.

**Table 1. Characterization results of A<sub>2</sub> + B<sub>3</sub>-type Hyperbranched Polyazomethines**

sample	M <sub>d,w</sub> (g mol <sup>-1</sup> )	M <sub>n</sub> (g mol <sup>-1</sup> )	PDI <sup>a</sup>	r <sup>b</sup>
PAM	19 600	13 300	1.47	1.53
PAMC 1	17 000	12 100	1.40	1.92
PAMC 2	18 400	12 200	1.51	1.92
PAMC 3	16 100	11 800	1.37	1.74
PAMC 4	19 500	12 900	1.51	1.83

<sup>a</sup>PDI = M<sub>w</sub>/M<sub>n</sub>. <sup>b</sup>r-Value was calculated as the integral ratio of characteristic protons on –CHO at 9.90–9.94 ppm and benzene near the amino group at 6.55–6.63 ppm to that of characteristic protons on –CH<sub>2</sub>– at 4.11–4.26 ppm. Polymer notation: C = cyclic, the numbers 1–4 indicate the cyclic times.

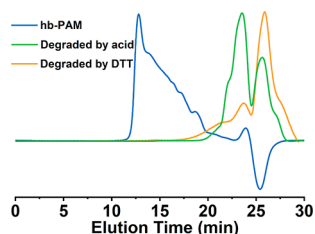


**Figure 4.** SEC trace of the hb-PAM and hb-PAM degraded by acid and DTT with a flow rate of 0.5 mL min<sup>-1</sup> in THF.

polymers based on imine bond had the characteristic of dynamic reversibility, which was controllable, and the polymer–monomer transition was able to undergo repeated cycles through regulating pH.

**3.3. Intramolecular Cyclization of hb-PAM and hb-PAMC 2–4.** Intramolecular cyclization occurs during the synthesis process of hyperbranched polymers via A<sub>2</sub> + B<sub>3</sub>

polycondensation. For the obtained hyperbranched polymers with A or B terminal groups, the *r* parameter can be defined to determine the degree of intramolecular cyclization.<sup>44</sup> In our previous work,<sup>45,46</sup> the quantitative relationship between cyclic structures and structural units for hyperbranched polymers was derived as

$$N_C = \begin{cases} N_{A_0} - N_{B_0} - N_{B_1} - N_{B_2} + N \\ 2 \times N_{B_0} + N_{B_1} - N_{A_0} - N_{A_1} + N \end{cases} \quad (1)$$

where *N*, *N<sub>C</sub>*, *N<sub>A0</sub>*, *N<sub>A1</sub>*, *N<sub>B0</sub>*, *N<sub>B1</sub>*, and *N<sub>B2</sub>* represents the number of total macromolecules, cyclic structures, A<sub>0</sub>, A<sub>1</sub>, B<sub>0</sub>, B<sub>1</sub>, and B<sub>2</sub> units, respectively. Noteworthy, A<sub>0</sub> and A<sub>1</sub> units refer to the structural units containing 0 and 1 A group, and B<sub>0</sub>, B<sub>1</sub>, and B<sub>2</sub> units refer to the structural units containing 0, 1, and 2 B groups (Figure 5). Eq 1 after the transformation is represented as the following equation:

$$N_{A_1} + N_{B_1} + 2N_{B_2} = N_{B_0} + N_{B_1} + N_{B_2} + 2N - 2N_C \quad (2)$$

(*N<sub>A1</sub>* + *N<sub>B1</sub>* + 2*N<sub>B2</sub>*) is total number of terminal groups and (*N<sub>B0</sub>* + *N<sub>B1</sub>* + *N<sub>B2</sub>*) means total number of B units. In Equ. 2, it can be found that the quantitative relationship between the end groups and B units closely correlated with the intramolecular cyclization. As a consequence, a parameter *r* is defined as the number proportion of total terminal groups to B units:

$$r = \frac{N_{A_1} + N_{B_1} + 2N_{B_2}}{N_{B_0} + N_{B_1} + N_{B_2}} = 1 + 2 \frac{N - N_C}{N_{B_0} + N_{B_1} + N_{B_2}} \quad (3)$$

Here, the *r* value is inversely proportional to degree of intramolecular cyclization. Through the integration of proton peak area in <sup>1</sup>H NMR spectra, the *r* value can be calculated. Table 1 summarizes that the *r* values of dynamic hyper-

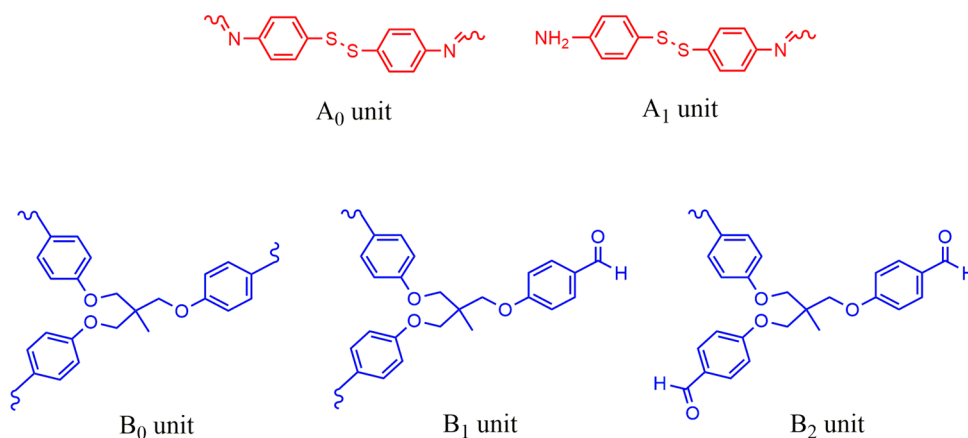


**Figure 5.** Division of topological units of the  $\text{A}_2$  monomer,  $\text{B}_3$  monomer, and hyperbranched polymer.

branched polymers hb-PAM and hb-PAMC 2–4 were all above 1.5, indicating that the intramolecular cyclization of the polymers was low. The  $r$  value of hb-PAM was lower than that of hb-PAMC 2–4. This was attributed to the fact that hb-PAMC 2–4 specimens were not purified, and they contained unreacted monomers leading to decreasing value of intramolecular cyclization. Moreover, the  $r$  values of hb-PAMC 2–4 did not change much, illustrating that the topological structure of the polymers remained nearly the same after repeatedly experiencing the reversible polymer–monomer transitions.

**3.4. Reductive Degradation of Hyperbranched Polyazomethine.** The DTT was utilized to trigger the degradation of the hb-PAM. The disulfide bonds have the characteristic of redox responsibility; therefore, the hb-PAM containing disulfide bonds could be dissociated by reductant. The cleavage of the polymer was monitored by SEC-MALLS. Figure 4 exhibits that the degradation behavior could be observed in the SEC trace. Compared to the peak of hb-PAM in the range from 12 to 20 min, a new peak of the degradation product appeared at 24 min, indicating that the hb-PAM was reduced by DTT.

**3.5. Mechanical Performance of the Cross-Linked Polyazomethine.** In a polymerization system, the higher the functionality of the reactants, the more likely gelation occurs. The hyperbranched polymers (hb-PAM) have abundant functional end groups. Therefore, they are exceptionally useful in curing systems, compared to low-functionality monomers. The hb-PAM was further cross-linked with PEA through Schiff base reaction to achieve self-healing polyazomethine (SH-PAM), as shown in Figure 6. The hb-PAM with amounts of aldehyde terminal groups facilitated the formation of three-dimensional cross-linked networks. Moreover, PEA 2000 served as a soft and hydrophobic segment, thus we could obtain a stretchable polymeric network. On the one hand, soft macromolecular chains contribute to enhance the flexibility and deformability. On the other hand, incorporating hydrophobic PEA segments into the cross-linked networks is to avoid hydrolysis of imine bond.

The mechanical performances of cross-linked polymers were greatly influenced by the ratio of monomers. Two kinds of SH-PAM (SH-PAM-1 and SH-PAM-2) were designed and prepared through adjusting the content of 4,4'-dithiodianiline and PEA, in which the total molar ratio of amino and aldehyde was maintained at 1:1. The typical stress–strain behaviors for SH-PAM-1 and SH-PAM-2 are shown in Figure 7a. SH-PAM-

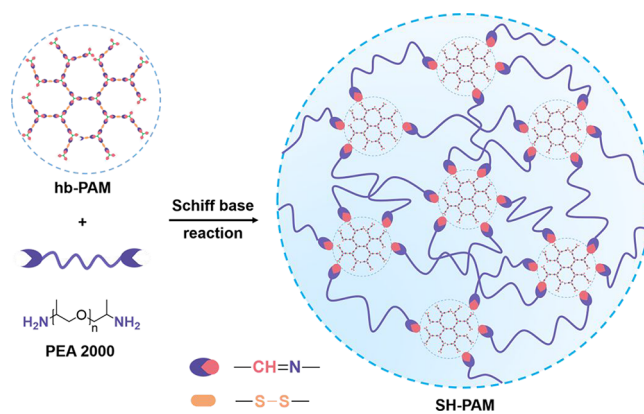


**Figure 6.** Schematic illustration of fabrication of self-healing polyazomethine (SH-PAM) elastomer cross-linked through Schiff base reaction.

1 presented maximum stress of 3.8 MPa and Young's modulus of 2.4 MPa, which were about 10 times higher than that of SH-PAM-2. While the SH-PAM-2 exhibited excellent stretchability with fracture strain of 510% (Figure 7b). The above results were for the reason that there were more rigid benzenes and conjugated structure as well as cross-linking points in SH-PAM-1. It is acknowledged that the molar ratio of  $\text{A}_2$  to  $\text{B}_3$  monomers controlled at 1:1 is more prone to obtain hyperbranched macromolecules with higher molecular weight,<sup>47</sup> indicating a larger number of terminal groups per polymeric chain. Additionally, in our previous work, an elastomer based on an imine bond cross-linked through PEA and FPME was reported with a peak stress of 0.79 MPa and fracture strain of 215%.<sup>9</sup> Obviously, SH-PAM-1 exhibited more robust mechanical property.

SH-PAM-1 was selected for further investigation. The cross-linked networks exhibited good elasticity and self-recovery capability. As shown in Figure 7c, loading–unloading cycle tests were performed with stretching to a strain of 50%. During the consecutive loading–unloading process, it showed obvious hysteresis, resulting from the energy dissipation. Subsequently, in cycle 2, the energy dissipation (within the loop of a cycle) was decreased, which could be ascribed to the enhancement of elastic deformation. After relaxing for 30 min, the sample was allowed to stretching again. It was found that the curve almost overlapped with that of cycle 1, indicating the sample fully recovered with the mechanical performance restored to its

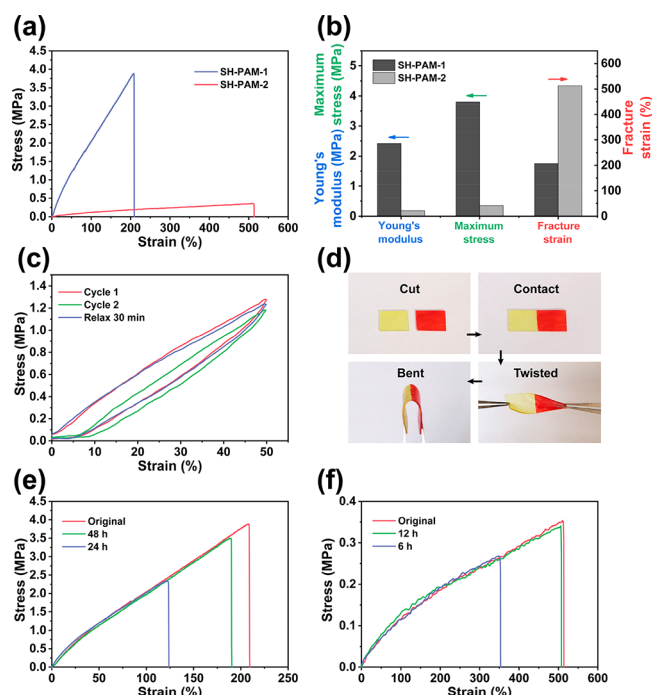


**Figure 7.** (a) Stress–strain curves of SH-PAM elastomers. (b) Young's modulus, maximum stress, and fracture strain of SH-PAM elastomers. (c) Recovery and cyclic loading–unloading curves of SH-PAM-1 to a strain of 50%. (d) Optical images showing self-healing behavior of SH-PAM-2. (e) Stress–strain curves of the original and self-healed elastomers at various healing times for (e) SH-PAM-1 and (f) SH-PAM-2. The tensile rates in (a), (c), (e), and (f) were 20 mm min<sup>-1</sup>.

original state. This phenomenon might be assigned to the synthetic action of imine and disulfide bonds with dynamic characteristics through bond breakage and reformation.

**3.6. Self-Healing Performance of the Cross-Linked Polyazomethine.** Driven by the reversibility of imine and disulfide bonds, the as-prepared SH-PAM elastomers were endowed with an excellent self-healing property. A piece of SH-PAM film specimen was cut from the middle, and one of them was dyed in red color. Then, they were brought into full contact. After healing, the sample could be subjected to be bending and twisting (Figure 7d). Then, the quantitative analysis of self-healing characteristic was conducted using uniaxial tensile tests at 25 °C (Figure 7e, f). The healing efficiency is deduced from the ratio of the fracture strain of the healed sample to that of the original sample. The calculations proved that the time-dependent healing efficiency of SH-PAM-1 was about 91% after healing for 48 h. Remarkably, the healing efficiency of SH-PAM-2 reached 99% after 12 h. The difference of healing efficiency between SH-PAM-1 and SH-PAM-2 was due to the flexibility of networks. SH-PAM-2 was softer than SH-PAM-1, leading to the molecular chains moving more easily. The ideal self-healing property results from the mobility of soft segments and synthetic effects of imine and disulfide bonds. The soft segments in the polymer networks facilitate the intimate contact between the broken surfaces. Therefore, the imine bonds could be reformed by the active aldehyde and amino groups generated at the scratched surfaces. Meanwhile, with the exchange and metathesis of imine, the system is in dynamic equilibrium.<sup>25</sup> For the reversibility of the reaction, there might be unreacted terminal

groups which could also form imine bond, contributing to self-healing process. Moreover, the aromatic disulfide undergoes instant exchange at room temperature,<sup>18</sup> leading to the healing of the cracked SH-PAM elastomers.

**3.7. Dual Responsiveness of Self-Healing Polyazomethine.** At the molecular levels, the pH and redox responsiveness of imine and disulfide bonds were investigated through the soluble hb-PAM. Therefore, undoubtedly, the cross-linked SH-PAM elastomers were provided with dual responsiveness. Figure 8 depicts that the soaking of SH-PAM-1

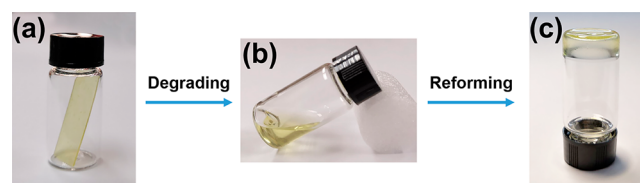


**Figure 8.** Optical photographs showing the responsiveness of SH-PAM-1: (a) the original, (b) soaking in the solution of AcOH or DTT, and (c) after evaporation of solvent.

in the solution of AcOH led to their complete dissociation. The solid state was transformed to liquid solution due to the cleavage of imine linkages and dissociation of cross-linked networks at low pH (Figure 8a, b). Interestingly, the cross-linked polymer could be prepared after adjusting pH and evaporating solvent at 80 °C (Figure 8c). Similarly, when DTT was added onto the surface of SH-PAM-1, the bulk polymer was completely decomposed. After exposure to air environments and volatilization of solvent, the film could be reformed due to the redox feature of disulfide bonds. Therefore, dual responsiveness of SH-PAM-1 could conveniently be achieved by common operations of dissociation and evaporation based on cleavage and polymerization of imine or disulfide bonds.

## CONCLUSIONS

Stretchable and self-healable elastomers with dual pH and redox responsibility were successfully synthesized, which were cross-linked through recyclable hyperbranched polymers based on reversible covalent bonds. The soluble hb-PAM exhibited the transitional behaviors between polymers and monomers. The polymer containing imine bonds could be decomposed into monomers at low pH, and the monomers could polymerize again to generate the hyperbranched polymer via regulating the reaction conditions. Moreover, this process could be repeated several times. The topological structures of the regenerated hb-PAM remained nearly the same after undergoing the reversible polymer–monomer transitions. Moreover, the hb-PAM was provided with redox cleavage ability triggered by DTT. Benefiting from the hb-PAM with multiple terminal groups, furthermore, the hb-PAM could be cross-linked with PEA through Schiff base reaction to achieve tough networks. Furthermore, the SH-PAM elastomers demonstrated excellent self-healing performance with a healing efficiency as high as 99% under ambient environment. Moreover, the SH-PAM elastomers exhibited remarkable dual responsiveness. The dynamic polymers may have promising applications in smart structures, programmable polymers, and soft electronics fields.

## ■ ASSOCIATED CONTENT

### Supporting Information

The Supporting Information is available free of charge at <https://pubs.acs.org/doi/10.1021/acsapm.9b01073>.

<sup>1</sup>H NMR of monomers and SEC traces of polymers (PDF)

## ■ AUTHOR INFORMATION

### Corresponding Authors

**Yansong Wang** – Key Laboratory of Optical System Advance Manufacturing Technology, Changchun Institute of Optics, Fine Mechanics and Physics, Chinese Academy of Sciences, Changchun 130033, China; Email: [wangyansong99@163.com](mailto:wangyansong99@163.com)

**Jie Kong** – MOE Key Laboratory of Materials Physics and Chemistry in Extraordinary Conditions, Shaanxi Key Laboratory of Macromolecular Science and Technology, School of Chemistry and Chemical Engineering, Northwestern Polytechnical University, Xi'an 710072, China; [orcid.org/0000-0002-9405-3204](https://orcid.org/0000-0002-9405-3204); Email: [kongjie@nwpu.edu.cn](mailto:kongjie@nwpu.edu.cn)

### Authors

**Xingyi Dai** – MOE Key Laboratory of Materials Physics and Chemistry in Extraordinary Conditions, Shaanxi Key Laboratory of Macromolecular Science and Technology, School of Chemistry and Chemical Engineering, Northwestern Polytechnical University, Xi'an 710072, China

**Yuzhang Du** – MOE Key Laboratory of Materials Physics and Chemistry in Extraordinary Conditions, Shaanxi Key Laboratory of Macromolecular Science and Technology, School of Chemistry and Chemical Engineering, Northwestern Polytechnical University, Xi'an 710072, China

**Yuncong Liu** – MOE Key Laboratory of Materials Physics and Chemistry in Extraordinary Conditions, Shaanxi Key Laboratory of Macromolecular Science and Technology, School of Chemistry and Chemical Engineering, Northwestern Polytechnical University, Xi'an 710072, China

**Nianxi Xu** – Key Laboratory of Optical System Advance Manufacturing Technology, Changchun Institute of Optics, Fine Mechanics and Physics, Chinese Academy of Sciences, Changchun 130033, China

**Yifan Li** – Mechanical and Construction Engineering, Faculty of Engineering and Environment, Northumbria University, Newcastle upon Tyne NE1 8ST, U.K.

**Dongzhi Shan** – Key Laboratory of Optical System Advance Manufacturing Technology, Changchun Institute of Optics, Fine Mechanics and Physics, Chinese Academy of Sciences, Changchun 130033, China

**Ben Bin Xu** – Mechanical and Construction Engineering, Faculty of Engineering and Environment, Northumbria University, Newcastle upon Tyne NE1 8ST, U.K.; [orcid.org/0000-0002-6747-2016](https://orcid.org/0000-0002-6747-2016)

Complete contact information is available at: <https://pubs.acs.org/doi/10.1021/acsapm.9b01073>

### Notes

The authors declare no competing financial interest.

## ■ ACKNOWLEDGMENTS

The work was supported by the National Natural Science Foundation of China through Grant 21374089, Shaanxi Natural Science Funds (Grant 2018JC-008, Distinguished

Young Scholars), and the Engineering and Physical Sciences Research Council (EPSRC) Grants EP/N007921/1 and EP/N032861/1.

## ■ REFERENCES

- (1) Rowan, S. J.; Cantrill, S. J.; Cousins, G. R.; Sanders, J. K.; Stoddart, J. F. Dynamic Covalent Chemistry. *Angew. Chem., Int. Ed.* **2002**, *41*, 898–952.
- (2) Nowak, P.; Saggiomo, V.; Salehian, F.; Colomb-Delsuc, M.; Han, Y.; Otto, S. Localized Template-Driven Functionalization of Nanoparticles by Dynamic Combinatorial Chemistry. *Angew. Chem., Int. Ed.* **2015**, *54*, 4192–4197.
- (3) Jin, Y.; Wang, Q.; Taynton, P.; Zhang, W. Dynamic Covalent Chemistry Approaches toward Macrocycles, Molecular Cages, and Polymers. *Acc. Chem. Res.* **2014**, *47*, 1575–1586.
- (4) Wojtecki, R. J.; Meador, M. A.; Rowan, S. J. Using the Dynamic Bond to Access Macroscopically Responsive Structurally Dynamic Polymers. *Nat. Mater.* **2011**, *10*, 14–27.
- (5) Ulrich, S. Growing Prospects of Dynamic Covalent Chemistry in Delivery Applications. *Acc. Chem. Res.* **2019**, *52*, 510–519.
- (6) Yuan, C. E.; Zhang, M. Q.; Rong, M. Z. Application of Alkoxyamine in Self-Healing of Epoxy. *J. Mater. Chem. A* **2014**, *2*, 6558–6566.
- (7) Fan, L. F.; Rong, M. Z.; Zhang, M. Q.; Chen, X. D. Repeated Intrinsic Self-Healing of Wider Cracks in Polymer via Dynamic Reversible Covalent Bonding Molecularly Combined with a Two-Way Shape Memory Effect. *ACS Appl. Mater. Interfaces* **2018**, *10*, 38538–38546.
- (8) Kovaricek, P.; Cebecauer, M.; Neburkova, J.; Barton, J.; Fridrichova, M.; Drogowska, K. A.; Cigler, P.; Lehn, J. M.; Kalbac, M. Proton-Gradient-Driven Oriented Motion of Nanodiamonds Grafted to Graphene by Dynamic Covalent Bonds. *ACS Nano* **2018**, *12*, 7141–7147.
- (9) Dai, X.; Du, Y.; Yang, J.; Wang, D.; Gu, J.; Li, Y.; Wang, S.; Xu, B. B.; Kong, J. Recoverable and Self-Healing Electromagnetic Wave Absorbing Nanocomposites. *Compos. Sci. Technol.* **2019**, *174*, 27–32.
- (10) Xin, Y.; Yuan, J. Y. Schiff's Base as a Stimuli-Responsive Linker in Polymer Chemistry. *Polym. Chem.* **2012**, *3*, 3045–3055.
- (11) Apostolides, D. E.; Sakai, T.; Patrickios, C. S. Dynamic Covalent Star Poly(ethylene glycol) Model Hydrogels: A New Platform for Mechanically Robust, Multifunctional Materials. *Macromolecules* **2017**, *50*, 2155–2164.
- (12) Deng, G.; Tang, C.; Li, F.; Jiang, H.; Chen, Y. J. M. Covalent Cross-Linked Polymer Gels with Reversible Sol-Gel Transition and Self-Healing Properties. *Macromolecules* **2010**, *43*, 1191–1194.
- (13) Ji, X.; Li, Z.; Liu, X.; Peng, H. Q.; Song, F.; Qi, J.; Lam, J. W. Y.; Long, L.; Sessler, J. L.; Tang, B. Z. A Functioning Macroscopic "Rubik's Cube" Assembled via Controllable Dynamic Covalent Interactions. *Adv. Mater.* **2019**, *31*, 1902365.
- (14) Xia, J.; Zhao, P.; Zheng, K.; Lu, C.; Yin, S.; Xu, H. Surface Modification Based on Diselenide Dynamic Chemistry: Towards Liquid Motion and Surface Bioconjugation. *Angew. Chem., Int. Ed.* **2019**, *58*, 542–546.
- (15) Pu, W.; Fu, D.; Wang, Z.; Gan, X.; Lu, X.; Yang, L.; Xia, H. Realizing Crack Diagnosing and Self-Healing by Electricity with a Dynamic Crosslinked Flexible Polyurethane Composite. *Adv. Sci.* **2018**, *5*, 1800101.
- (16) Wu, S.; Li, J.; Zhang, G.; Yao, Y.; Li, G.; Sun, R.; Wong, C. Ultrafast Self-Healing Nanocomposites via Infrared Laser and Their Application in Flexible Electronics. *ACS Appl. Mater. Interfaces* **2017**, *9*, 3040–3049.
- (17) Duan, X.; Chen, H.; Fan, L.; Kong, J. Drug Self-Assembled Delivery System with Dual Responsiveness for Cancer Chemotherapy. *ACS Biomater. Sci. Eng.* **2016**, *2*, 2347–2354.
- (18) Rekondo, A.; Martin, R.; Ruiz de Luzuriaga, A.; Cabañero, G.; Grande, H. J.; Odriozola, I. Catalyst-Free Room-Temperature Self-Healing Elastomers Based on Aromatic Disulfide Metathesis. *Mater. Horiz.* **2014**, *1*, 237–240.

- (19) Xu, W.; Huang, L.-B.; Hao, J. H. Fully Self-Healing and Shape-Tailorable Triboelectric Nanogenerators Based on Healable Polymer and Magnetic-Assisted Electrode. *Nano Energy* **2017**, *40*, 399–407.
- (20) Chakma, P.; Konkolewicz, D. Dynamic Covalent Bonds in Polymeric Materials. *Angew. Chem., Int. Ed.* **2019**, *58*, 9682–9695.
- (21) Debnath, S.; Ujjwal, R. R.; Ojha, U. Self-Healable and Recyclable Dynamic Covalent Networks Based on Room Temperature Exchangeable Hydrazide Michael Adduct Linkages. *Macromolecules* **2018**, *51*, 9961–9973.
- (22) Feng, Z.; Hu, J.; Zuo, H.; Ning, N.; Zhang, L.; Yu, B.; Tian, M. Photothermal-Induced Self-Healable and Reconfigurable Shape Memory Bio-Based Elastomer with Recyclable Ability. *ACS Appl. Mater. Interfaces* **2019**, *11*, 1469–1479.
- (23) Xin, Y.; Peng, H.; Xu, J.; Zhang, J. Ultrauniform Embedded Liquid Metal in Sulfur Polymers for Recyclable, Conductive, and Self-Healable Materials. *Adv. Funct. Mater.* **2019**, *29*, 1808989.
- (24) Diesendruck, C. E.; Peterson, G. I.; Kulik, H. J.; Kaitz, J. A.; Mar, B. D.; May, P. A.; White, S. R.; Martinez, T. J.; Boydston, A. J.; Moore, J. S. Mechanically Triggered Heterolytic Unzipping of a Low-Ceiling-Temperature Polymer. *Nat. Chem.* **2014**, *6*, 623–628.
- (25) Belowich, M. E.; Stoddart, J. F. Dynamic Imine Chemistry. *Chem. Soc. Rev.* **2012**, *41*, 2003–2024.
- (26) Meyer, C. D.; Joiner, C. S.; Stoddart, J. F. Template-Directed Synthesis Employing Reversible Imine Bond Formation. *Chem. Soc. Rev.* **2007**, *36*, 1705–1723.
- (27) Hu, B.; Zhu, X.; Chen, X.; Pan, L.; Peng, S.; Wu, Y.; Shang, J.; Liu, G.; Yan, Q.; Li, R.-W. A Multilevel Memory Based on Proton-Doped Polyazomethine with an Excellent Uniformity in Resistive Switching. *J. Am. Chem. Soc.* **2012**, *134*, 17408–17411.
- (28) Pandey, P.; Katsoulidis, A. P.; Eryazici, I.; Wu, Y.; Kanatzidis, M. G.; Nguyen, S. T. Imine-Linked Microporous Polymer Organic Frameworks. *Chem. Mater.* **2010**, *22*, 4974–4979.
- (29) Ji, S.; Cao, W.; Yu, Y.; Xu, H. Visible-Light-Induced Self-Healing Diselenide-Containing Polyurethane Elastomer. *Adv. Mater.* **2015**, *27*, 7740–7745.
- (30) Zhang, H.; Wu, Y.; Yang, J.; Wang, D.; Yu, P.; Lai, C. T.; Shi, A. C.; Wang, J.; Cui, S.; Xiang, J.; Zhao, N.; Xu, J. Superstretchable Dynamic Polymer Networks. *Adv. Mater.* **2019**, *31*, 1904029.
- (31) Liu, J.; Zhang, X.; Chen, X.; Qu, L.; Zhang, L.; Li, W.; Zhang, A. Stimuli-Responsive Dendronized Polymeric Hydrogels through Schiff-Base Chemistry Showing Remarkable Topological Effects. *Polym. Chem.* **2018**, *9*, 378–387.
- (32) Ban, Q.; Sun, W.; Kong, J.; Wu, S. Hyperbranched Polymers with Controllable Topologies for Drug Delivery. *Chem. - Asian J.* **2018**, *13*, 3341–3350.
- (33) Zheng, W.; Chen, L. J.; Yang, G.; Sun, B.; Wang, X.; Jiang, B.; Yin, G. Q.; Zhang, L.; Li, X.; Liu, M.; Chen, G.; Yang, H. B. Construction of Smart Supramolecular Polymeric Hydrogels Cross-Linked by Discrete Organoplatinum (II) Metallacycles via Post-Assembly Polymerization. *J. Am. Chem. Soc.* **2016**, *138*, 4927–4937.
- (34) Wang, C.; Wang, G.; Wang, Z.; Zhang, X. A pH-Responsive Superamphiphile Based on Dynamic Covalent Bonds. *Chem. - Eur. J.* **2011**, *17*, 3322–3325.
- (35) Sagara, Y.; Karman, M.; Verde-Sesto, E.; Matsuo, K.; Kim, Y.; Tamaoki, N.; Weder, C. Rotaxanes as Mechanochromic Fluorescent Force Transducers in Polymers. *J. Am. Chem. Soc.* **2018**, *140*, 1584–1587.
- (36) Kong, J.; Schmalz, T.; Motz, G.; Mueller, A. H. E. Novel Hyperbranched Ferrocene-Containing Poly(boro)carbosilanes Synthesized via a Convenient “A<sub>2</sub>+B<sub>3</sub>” Approach. *Macromolecules* **2011**, *44*, 1280–1291.
- (37) Chen, H.; Kong, J. Hyperbranched Polymers from A<sub>2</sub> + B<sub>3</sub> Strategy: Recent Advances in Description and Control of Fine Topology. *Polym. Chem.* **2016**, *7*, 3643–3663.
- (38) Tian, W.; Li, X.; Wang, J. Supramolecular Hyperbranched Polymers. *Chem. Commun.* **2017**, *53*, 2531–2542.
- (39) Skidin, D.; Faizy, O.; Kruger, J.; Eisenhut, F.; Jancarik, A.; Nguyen, K. H.; Cuniberti, G.; Gourdon, A.; Moresco, F.; Joachim, C. Unimolecular Logic Gate with Classical Input by Single Gold Atoms. *ACS Nano* **2018**, *12*, 1139–1145.
- (40) Zhang, X.; Soh, S. Performing Logical Operations with Stimuli-Responsive Building Blocks. *Adv. Mater.* **2017**, *29*, 1606483.
- (41) Sambe, L.; de La Rosa, V. R.; Belal, K.; Stoffelbach, F.; Lyskawa, J.; Delattre, F.; Bria, M.; Cooke, G.; Hoogenboom, R.; Woisel, P. Programmable Polymer-Based Supramolecular Temperature Sensor with a Memory Function. *Angew. Chem., Int. Ed.* **2014**, *53*, 5044–5048.
- (42) Kragt, A. J. J.; Broer, D. J.; Schenning, A. P. H. J. Easily Processable and Programmable Responsive Semi-Interpenetrating Liquid Crystalline Polymer Network Coatings with Changing Reflectivities and Surface Topographies. *Adv. Funct. Mater.* **2018**, *28*, 1704756.
- (43) Ogden, W. A.; Guan, Z. Recyclable, Strong, and Highly Malleable Thermosets Based on Boroxine Networks. *J. Am. Chem. Soc.* **2018**, *140*, 6217–6220.
- (44) Chen, H.; Jia, J.; Duan, X.; Yang, Z.; Kong, J. Reduction-Cleavable Hyperbranched Polymers with Limited Intramolecular Cyclization via Click Chemistry. *J. Polym. Sci., Part A: Polym. Chem.* **2015**, *53*, 2374–2380.
- (45) Chen, H.; Kong, J. Terminal Index: A New Way for Precise Description of Topologic Structure of Highly Branched Polymers Derived from A<sub>2</sub> + B<sub>3</sub> Stepwise Polymerization. *J. Phys. Chem. B* **2014**, *118*, 3441–3450.
- (46) Chen, H.; Zhang, S.; Kong, J. Topological Analysis and Intramolecular Cyclic Feature Evaluation of Polymers Derived from A<sub>m</sub> + B<sub>n</sub> Step-Growth Polymerization. *Polym. Chem.* **2015**, *6*, 909–916.
- (47) Lin, Q.; Long, T. E. Polymerization of A<sub>2</sub> with B<sub>3</sub> Monomers: A Facile Approach to Hyperbranched Poly(aryl ester)s. *Macromolecules* **2003**, *36*, 9809–9816.